

Seasonal Variation of Thermospheric Composition Observed by NASA GOLD

Liying Qian¹, Quan Gan², Wenbin Wang³, Xuguang Cai⁴, Richard W Eastes⁵, and Jia Yue⁶

¹National Center for Atmospheric Research (UCAR)

²Laboratory for Atmospheric and Space Physics (LASP), University of Colorado Boulder

³HAO/NCAR

⁴U of Colorado, Boulder

⁵Laboratory for Atmospheric and Space Physics

⁶Goddard Space Flight Center

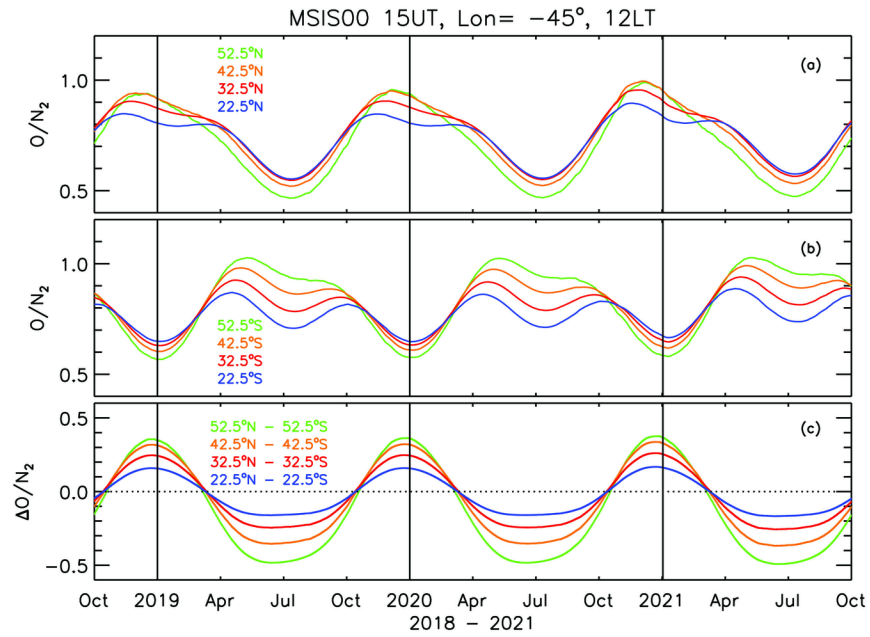
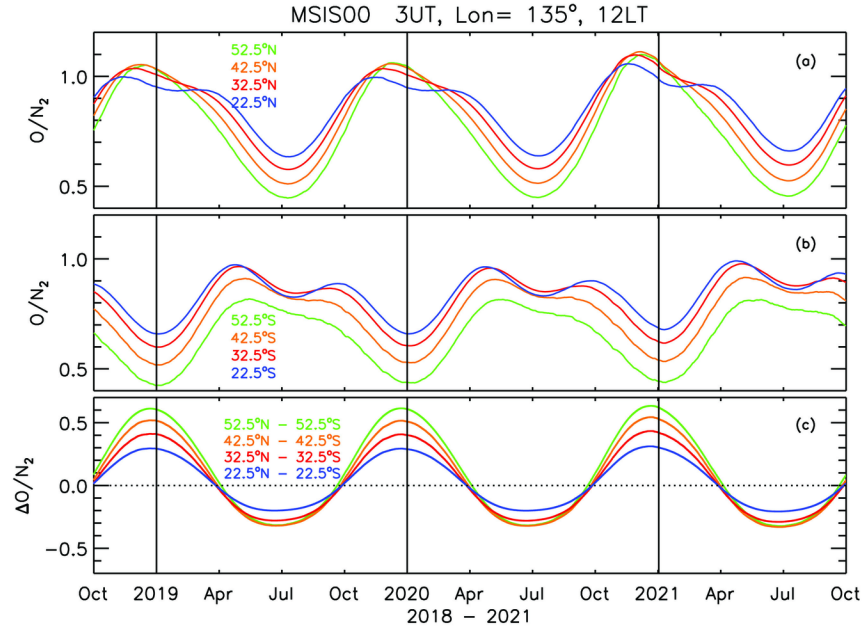
November 21, 2022

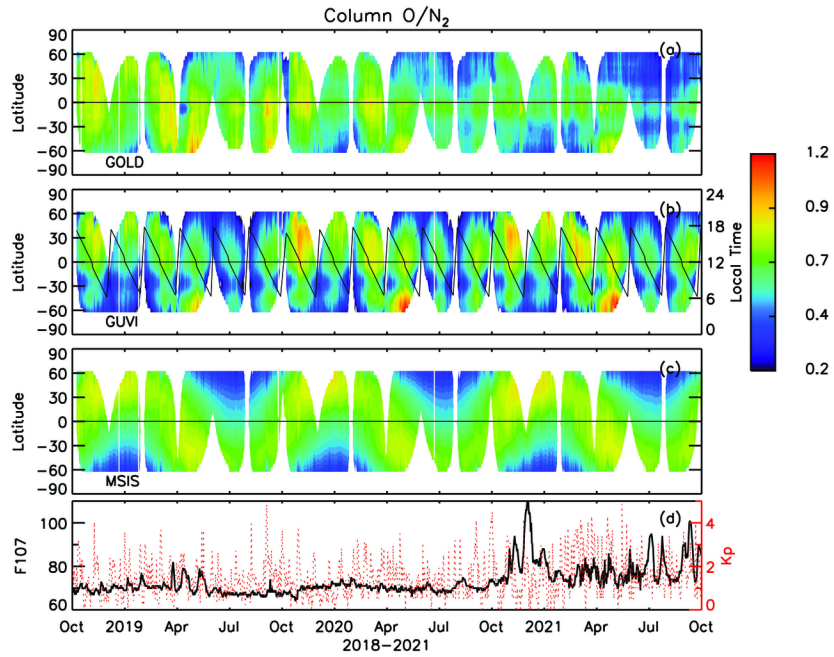
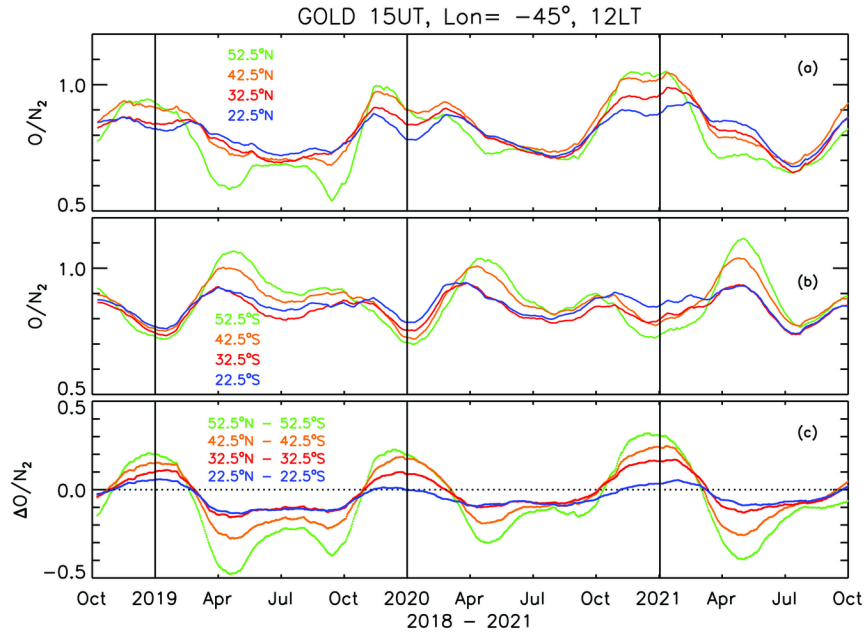
Abstract

We examine characteristics of the seasonal variation of thermospheric composition using column number density ratio $[O]/N_2$ observed by the NASA Global Observations of Limb and Disk (GOLD) mission from low-mid to mid-high latitudes. We found that the $[O]/N_2$ seasonal variation is hemispherically asymmetric: in the southern hemisphere, it exhibits the well-known annual and semiannual pattern, with highs near the equinoxes, and primary and secondary lows near the solstices. In the northern hemisphere, it is dominated by an annual variation, with a minor semiannual component with the highs shifting towards the wintertime. We also found that the durations of the December and June solstice seasons in terms of $[O]/N_2$ are highly variable with longitude. Our hypothesis is that ion-neutral collisional heating in the equatorial ionization anomaly region, ion drag, and auroral Joule heating play substantial roles in this longitudinal dependency. Finally, the rate of change in $[O]/N_2$ from one solstice season to the other is dependent on latitude, with more dramatic changes at higher latitudes.

Hosted file

essoar.10510966.1.docx available at <https://authorea.com/users/521310/articles/596494-seasonal-variation-of-thermospheric-composition-observed-by-nasa-gold>





Seasonal Variation of Thermospheric Composition Observed by NASA GOLD

Liyang Qian¹, Quan Gan², Wenbin Wang¹, Xuguang Cai², Richard Eastes², Jia Yue^{3,4}

¹High Altitude Observatory, National Center for Atmospheric Research, USA

²Laboratory for Atmospheric and Space Physics, University of Colorado, Boulder, CO, USA

³Goddard Space Flight Center, NASA

⁴Catholic University of America

Abstract. We examine characteristics of the seasonal variation of thermospheric composition using column number density ratio O/N_2 observed by the NASA Global Observations of Limb and Disk (GOLD) mission from low-mid to mid-high latitudes. We found that the O/N_2 seasonal variation is hemispherically asymmetric: in the southern hemisphere, it exhibits the well-known annual and seminal pattern, with highs near the equinoxes, and primary and secondary lows near the solstices. In the northern hemisphere, it is dominated by an annual variation, with a minor semiannual component with the highs shifting towards the wintertime. We also found that the durations of the December and June solstice seasons in terms of O/N_2 are highly variable with longitude. Our hypothesis is that ion-neutral collisional heating in the equatorial ionization anomaly region, ion drag, and auroral Joule heating play substantial roles in this longitudinal dependency. Finally, the rate of change in O/N_2 from one solstice season to the other is dependent on latitude, with more dramatic changes at higher latitudes.

Plain Language Summary. We study how the amount of atmosphere constituent in the Earth's thermosphere change over a year at low-mid to mid-high latitudes using the data measured by the NASA Global Observations of Limb and Disk (GOLD) mission. The main constituents in the thermosphere are atomic oxygen (O) and molecular nitrogen (N_2). The ratio of O and N_2 , O/N_2 , is a common way to measure the relative abundance of these two constituents. The GOLD mission uses instruments aboard on a geostationary satellite to observe O/N_2 . We found that how O/N_2 changes over a year is different in the northern and southern hemispheres. In the southern hemisphere, it has an annual and seminal pattern, with high O/N_2 near the equinoxes, and primary and secondary lows near the solstices. In the northern hemisphere, it is mainly an annual pattern, with a minor semiannual component. The semiannual component has high O/N_2 values shifting away from the equinoxes towards the wintertime. We also found that whether O/N_2 is larger in one hemisphere or the other highly depends on longitude.

1. Introduction

Annual and semiannual variations are one of the most prevalent climatological

features in both the thermosphere and ionosphere (e.g., Rishbeth et al., 2000; Bowman, 2004; Emmert and Picone, 2010; Zhang et al., 2005, 2010; Qian et al., 2009, 2013; Burns et al., 2012; Pillinski and Crowley, 2015). Paetzold and Zschorner (1961) first reported the annual/semiannual variations in thermosphere mass density through analysis of satellite drag data. They found that global mean mass density in the thermosphere has a primary minimum near the June solstice, a secondary minimum near the December solstice, and maxima near the equinoxes. Bowman (2004) found that the amplitudes and phases of the annual/semiannual variations showed significant changes from year to year and had an altitude dependence.

The Earth is in an elliptical orbit around the Sun. This introduces a $\sim 7\%$ difference in the solar irradiance that reaches the Earth’s thermosphere between early July (aphelion) and early January (perihelion), which causes an annual variation in the thermosphere and ionosphere (Zeng et al., 2008). Fuller-Rowell (1998) proposed the “thermospheric spoon” mechanism for the semiannual variation. The summer-to-winter circulation causes stronger mixing of the thermosphere during the solstices, and thus smaller neutral density scale height and less mass density.

However, the annual/semiannual variation driven by the sun-earth distance and “thermospheric spoon” is not sufficient to account for the magnitudes of the observed annual/semiannual variation in thermosphere mass density. Qian et al. (2009) found that a seasonally varying eddy diffusion, representing contributions from the lower atmospheric forcing, was needed at the lower boundary of the Thermosphere-Ionosphere-Electrodynamics General Circulation Model (TIE-GCM) (Roble et al., 1988; Richmond et al., 1992; Qian et al., 2014) to bring the simulated mass density to be in better agreement with satellite drag data. However, since the satellite drag data was a globally averaged dataset, this seasonally varying eddy diffusion was applied globally without considering its potential latitudinal variability.

Lei et al. (2012) examined annual and semiannual variations in thermosphere density observed by Challenging Minisatellite Payload (CHAMP) (Reigber et al., 2002) and Gravity Recovery and Climate Experiment (GRACE) (Tapley et al., 2004) satellites. They found that annual variations become dominant in the southern hemisphere whereas semiannual variations are seen at all latitudes, with amplitudes about 15–20% of the annual mean.

Yue et al. (2019) analyzed the Global Ultraviolet Imager (GUVI) limb measurements onboard the Thermosphere Ionosphere Mesosphere Energetics and Dynamics (TIMED) satellite and found that the ratio of O and N_2 number density (O/N_2) in the thermosphere shows a strong annual variation at midlatitudes and a clear semiannual variation at lower latitudes. O/N_2 , or the column integrated ratio of O and N_2 (O/N_2), are a measure of the relative abundance of O and N_2 in the thermosphere. They are often used to represent thermosphere composition.

Mass density measured by CHAMP and GRACE, and O/N_2 measured by GUVI limb observations provide annual and semiannual variations at different latitudes, but it is not possible to separate variations due to local time and longitude of the observations from the seasonal and latitudinal variations.

The NASA Global Observations of Limb and Disk (GOLD) mission has observed thermosphere and ionosphere in a geostationary orbit from October 2018 to present. Column integrated ratios O/N_2 are derived from daytime disk measurements of O 135.6 nm and N_2 Lyman-Birge-Hopfield (LBH) band emission radiance (140.0 – 150.0 nm). GOLD observes about one third of the earth’s upper atmosphere ($\sim 120^\circ\text{W} - 20^\circ\text{E}$, $60^\circ\text{N} - 60^\circ\text{S}$) simultaneously. The GOLD O/N_2 data allow us to study seasonal variations accurately by separating temporal and spacial variations. In this paper, we compare GOLD O/N_2 data with O/N_2 derived from GUVI disk measurements and estimated using the NRLMSISE-00 empirical model (Picone et al., 2002) for consistency, focusing on the seasonal time scale. We then characterize the latitudinal variability of the seasonal variations of GOLD O/N_2 by examining O/N_2 at a fixed local time and a fixed longitude.

Section 2 briefly describes GOLD and GUVI O/N_2 data; section 3 presents comparison results and characteristics of the seasonal variations of O/N_2 at noon revealed in GOLD data; section 4 discusses the results; and section 5 concludes the study.

1. Data

NASA GOLD O/N_2 data

The GOLD instruments are onboard the SES-14 communication satellite, which was launched on January 25, 2018. The SES-14 satellite is in a geostationary orbit over 47.5°W . The GOLD instruments are Far Ultraviolet (FUV) imagers, which consist of two similar and independent channels (Channels A and B) (Eastes et al., 2017, 2020). The GOLD imagers scan a fixed geographic region with a maximum longitude range from 120°W to 20°E and a latitude range from 60°S to 60°N . During the daytime, it observes Earth’s airglow emissions from ~ 134 to 162 nm with a spectral resolution of 0.2 nm. At night, it observes O 135.6 nm emission with a spectral resolution of 0.4 nm. O/N_2 referenced at a fixed N_2 column density of $1 \times 10^{17} \text{cm}^{-2}$ is derived from the daytime disk O 135.6 nm and N_2 LBH emission radiance, with a temporal resolution of 30 minutes (Correira et al., 2021).

Note that the O 135.6 nm emission on the dayside is not purely thermospheric emission because it can also be produced by the radiative recombination of O^+ and thus cause error in derived O/N_2 , which may not be negligible, especially at the crest of the equatorial ionization anomaly (EIA). Correira et al. (2021) estimated that the error in the derived GOLD O/N_2 due to radiative recombination of O^+ is $1\% - 2\%$ for a wide range of solar zenith and emission angles during periods of low solar and geomagnetic activity (the first few years of the GOLD mission), but the error will become larger as

geomagnetic active increases during Solar Cycle 25, with a potential of reaching $\sim 10\%$ – 20% . In addition, sometimes GOLD O/N_2 in the equatorial region is uncharacteristically large (Figure 1a). This is an artifact introduced when the current flat-field correction is unable to correctly compensate for detector degradation where the aurora and the high-latitude, sunlit limb –which is also seen during nightside observations near solstices, are observed. As a result, we avoid the equatorial region and examine the seasonal variations in the latitude region from 20° to 60° (low-mid to mid-high latitudes) in this study. In addition, for the version 3 data used in this study, a linear trend of -7% per year in the O/N_2 has been identified. This decrease is attributed to the flat-field correction to remove date dependent, spatial variations in sensitivity. We remove this linear trend in the GOLD O/N_2 when we study the characteristics of seasonal variations (Figure 2). A more robust flat-field correction has been developed and will be used for the next data update. GOLD O/N_2 are available online at <http://gold.cs.ucf.edu/search/>.

NASA TIMED/GUVI O/N_2 data

The TIMED satellite was launched on December 7, 2001. The GUVI instrument aboard the satellite provides images and spectra of FUV emissions from the thermosphere in the wavelengths between 115 and 180 nm on both dayside and nightside (Paxton et al., 1999; Christensen et al., 2003). The GUVI disk dayglow data at O 135.6 nm and N_2 LBH (140-150 nm) have been used to derive O/N_2 referenced at a fixed N_2 column density of $1 \times 10^{17} \text{cm}^{-2}$ (Zhang et al., 2004). GUVI O/N_2 are available at: http://guvitimed.jhuapl.edu/data_products.

1. Results

We first compare O/N_2 from GOLD, GUVI, and NRLMSISE-00, focusing on the seasonal time scale. As mentioned earlier, GOLD is on a geosynchronous orbit whereas TIME/GUVI is on a sun-synchronous orbit. To conduct meaningful comparisons, we obtain O/N_2 from GOLD, GUVI, and NRLMSISE-00 at the intersection of the GOLD field of view (FOV) and GUVI orbits: (1) run NRLMSISE-00 globally using a resolution of 5° latitude by 5° longitude by 2 km, in the altitude range of 100 – 450 km, with a time step of one hour; (2) for each 5° latitude bin, obtain O/N_2 observed concurrently by GOLD and GUVI at the intersection of the GOLD FOV and GUVI orbits for each day, and then calculate daily mean O/N_2 ; calculate the corresponding NRLMSISE-00 daily mean O/N_2 at the intersection of the GOLD FOV and GUVI orbits.

Figures 1a -1c are the daily mean O/N_2 obtained from GOLD, GUVI, and NRLMSISE-00, respectively, in the latitude range of $60^\circ\text{S} - 60^\circ\text{N}$, from October 2018 to October 2021. The zig-zag black line in Figure 1b shows the GUVI observation local times, which are also the local times for the GOLD and NRLMSISE-00 O/N_2 in Figures 1a and 1c. Figure 1d shows the $F10.7$ (black) and Kp (red) indices for this period. Daily $F10.7$ and daily Ap were used as input for NRLMSISE-00. Daily Kp is plotted in Figure 1d to show small geomagnetic variations from October 2018 to October 2021 more clearly

(Ap is proportional to the exponential of Kp). Note that O/N_2 from GOLD is systematically higher than NRLMSISE-00, whereas O/N_2 from GUVI is systematically lower than NRLMSISE-00. GOLD O/N_2 in Figure 1a was divided by 1.25 and GUVI O/N_2 in Figure 1b was multiplied by 1.25 for comparison purpose. It is not clear what have caused this systematic difference among the datasets. One of the possible reasons is the difference in the altitude registration among GOLD, GUVI, and NRLMSISE-00 to where the N_2 column number density is $1 \times 10^{17} \text{ cm}^{-2}$. This systematic difference is less of a concern when the focus is on seasonal variability.

Note that GUVI O/N_2 is low in the latitude range $\sim 10^\circ\text{S} - 40^\circ\text{S}$. This is an artifact due to impact of the MeV particles from the Southern Atlantic Anomaly (SAA) on the GUVI instruments.

A predominant annual variation with a summer low and winter high in O/N_2 at higher latitudes (greater than $\sim 30^\circ$) is a consistent feature in all three datasets. The winter high O/N_2 at higher latitudes in one hemisphere transitions to the winter high at higher latitudes in the other hemisphere through the equinoxes and the lower latitudes, giving rise to seasonal variations at different latitudes with different annual and semiannual components. These overall seasonal/latitudinal patterns of O/N_2 are consistent in the three datasets.

An interesting feature is that multi-day variations consistent with geomagnetic forcing (Qian and Solomon, 2011), shown as shorter-term variability in Figure 1a and Figure 1b, are evident in both GOLD and GUVI datasets but are often missing or weaker in NRLMSISE-00. NRLMSISE-00 uses empirical parameterization to estimate geomagnetic forcing effects, so it is difficult to accurately represent effects of a specific geomagnetic disturbance.

We now examine the latitudinal variability of the seasonal variations of GOLD O/N_2 at a fixed local time and a fixed longitude. Figure 2 shows the seasonal variations at 45°W and 12:00 LT, at four latitudes in each hemisphere: 52.5°N (green), 42.5°N (brown), 32.5°N (red), and 22.5°N (blue) in Figure 2a, and 52.5°S (green), 42.5°S (brown), 32.5°S (red), and 22.5°S (blue) in Figure 2b. We also calculate O/N_2 difference between a northern hemisphere latitude and its corresponding southern hemisphere latitude. Figure 2c shows the O/N_2 differences between pairs of northern and southern latitudes at 52.5° (green), 42.5° (brown), 32.5° (red), and 22.5° (blue). We define the time period when the O/N_2 difference is positive as *the December solstice season*, and the period when it is negative as *the June solstice season*. The vertical black lines in Figure 2 show the beginning of years 2019, 2020, and 2021.

There are three distinct characteristics in the seasonal variations:

- (1) There is a clear hemispheric asymmetry in the seasonal variations. In the southern hemisphere, the seasonal variations exhibit the well-known annual and seminal pattern, with the highs near the equinoxes, and primary and secondary lows near the solstices. The March equinox highs occur earlier at lower latitudes than at higher latitudes, whereas the September equinox highs occur earlier at

higher latitudes than at lower latitudes. In the northern hemisphere, however, the seasonal pattern is dominated by an annual variation. There is a small semiannual component, but the highs of the semiannual component shift earlier in the case of the March equinox and shift later in the case of the September equinox towards the wintertime, with a larger shift at higher latitudes. In both hemispheres, the annual and semiannual amplitudes increase with latitude.

(2) The December solstice season is much shorter than the June solstice season (Figure 2c). The average durations for the December solstice season and the June solstice season during this period (October 2018 – September 2021) are 122 days and 243 days, respectively.

(3) The O/N_2 difference in Figure 2c increases as latitude increases in both the December and June solstice seasons, but the transition times between the two solstice seasons do not change much with latitudes except at 22.5° when the O/N_2 difference is very small.

We further examine whether these characteristics of the seasonal variations from GOLD O/N_2 are present in the corresponding NRLMSISE-00 O/N_2 . Note that the local time of GUVI O/N_2 varies from day to day due to orbital precession, and the longitudes of GUVI O/N_2 change from orbit to orbit on each day, so GUVI O/N_2 is not used here. Figure 3 is the same as Figure 2 except that the results are from NRLMSISE-00.

NRLMSISE-00 O/N_2 shows seasonal characteristics that are consistent with those shown in GOLD O/N_2 :

(1) There is a hemispheric asymmetry in the seasonal variations of NRLMSISE-00 O/N_2 that is consistent with that in GOLD O/N_2 .

(2) The December solstice season for NRLMSISE-00 O/N_2 is also much shorter than the June solstice season. The average durations for the December and June solstice seasons during this data period are 145 days and 220 days, respectively.

(3) The O/N_2 differences in Figure 3c also increases as latitude increases in both the December and June solstice seasons, and the transition times between the two solstice seasons also do not change much with latitude.

The December solstice season is shorter in duration than the June solstice season at all latitudes in both GOLD and NRLMSISE-00 O/N_2 (Figures 2c and 3c). To find out whether the hemispheric asymmetry and this duration difference between the December and June solstice seasons are global phenomena, we analyze the NRLMSISE-00 results at 135° E. Note that 135° E is chosen because the locations of the magnetic equator at these longitudes are very different. Also note that we use NRLMSISE-00 O/N_2 since 135° E is not in the GOLD field of view. Figure 4 is the same as Figure 3 except that the results are for 135° E. We notice that the hemispheric asymmetry in the seasonal variations at 135° E is consistent with the results at 45° W, with well-defined annual/semiannual variations in the southern hemisphere but dominant annual variations in the

northern hemisphere. However, there are two significantly different aspects between the results at 135°E and 45°W:

1. There is significant difference in the latitudinal variation of O/N_2 in the southern hemisphere between the results at 135°E and 45°W. During the June solstice season, O/N_2 increases with latitude at 45°W; at 135°E, the largest O/N_2 is at 32.5°S, with O/N_2 decreasing with latitude from 32.5°S to 52.5°S.
2. Compared to the results at 45°W, the duration of the December solstice season (187 days) at 135°E has increased significantly and become longer than the June solstice season (178 days); the magnitudes of the O/N_2 differences have also switched between the December and June solstice seasons compared to the ones at 45°W (Figures 3c & 4c).

These differences demonstrate that the latitude region of the winter high O/N_2 , the durations of the June and December solstice seasons, and the magnitudes of the hemispheric O/N_2 difference, are all highly dependent on longitude, presumably due to a longitudinal dependence in the seasonal variation forcing.

1. Discussion

Hemispheric Asymmetry

Figure 6 of Yue et al. (2019) shows GUVI limb O/N_2 in the lower (8.4×10^{-4} Pa) and upper (6.35×10^{-6} Pa) thermosphere in five latitude zones (30–60°N, 10–30°N, 10°S to 10°N, 30–10°S, and 60–30°S). In both the lower and upper thermosphere, O/N_2 in the latitude zones 10–30°N and 30–10°S exhibit a hemispheric asymmetry similar to the hemispheric asymmetry in the GOLD and NRLMSISE-00 O/N_2 : at 30–10°S, the highs of the semiannual component is near the equinoxes; at 10–30°N, the highs of the semiannual component shift away from the equinoxes towards the wintertime, although it is difficult to discern whether the annual component is more dominant. In both the lower and upper thermosphere, the seasonal variation of O/N_2 in the latitude zones 30–60°N and 60–30°S are dominated by an annual variation, with only a remnant semiannual component. It is difficult to discern the semiannual component at 60–30°S, but at 30–60°N, a semiannual component is evident in 2006. The high O/N_2 of this northern hemisphere semiannual component also shifts away from the equinoxes towards the wintertime, consistent with those in GOLD O/N_2 . Note that these density ratio O/N_2 values are not O/N_2 as in the case of GOLD, but both Yue et al. (2019) and Yu et al. (2020) found that the annual and semiannual variations in composition have a constant phase with altitude throughout the thermosphere.

Longitudinal Dependency of the Equinox Transition

Note that there is no “equinox season” in Figures 2c, 3c, and 4c when the composition of pairs of northern and southern latitudes in the latitude region of 20° – 60° is the same. O/N_2 is either higher in one hemisphere or the other. Therefore, as far as O/N_2 is concerned, there is only the December

solstice season or June solstice season, and the transition between the December solstice and June solstice seasons, *the equinox transition*, has a time scale on the order of one day since the data temporal resolution is one day in these figures. The timings of the equinox transition, which determine the durations of the December solstice and June solstice seasons, are highly variable with longitude. In addition, the magnitudes of the hemispheric O/N_2 differences, and the winter downwelling zone of the summer-to-winter circulation, which determines where O/N_2 maximizes, are also longitudinally dependent.

Rishbeth and Müller-Wodarg (1999) found that the latitude of the downwelling regions varies with longitude because the thermospheric circulation is influenced by the high-latitude energy inputs, which are related to the geometry of the Earth’s magnetic field. Qian et al. (2016a) found that the latitude of the downwelling regions also varies with longitude because of the ion-neutral collisional heating in the equatorial ionization anomaly (EIA) region and ion drag. The longitudinal dependencies in the EIA ion-neutral collisional heating, ion drag, and auroral Joule heating result in a strong longitudinal variation of O/N_2 observed by GUVI (Qian et al., 2016b). Our hypothesis is that the EIA ion-neutral collisional heating, ion drag, and auroral Joule heating play substantial roles in determining the longitudinal dependency of the durations of the June and December solstice seasons and the magnitudes of the O/N_2 differences during the two solstice seasons. Further studies are needed to fully uncover the physical processes by which this dependence occurs.

Note that the results shown in Figures 3 & 4 are at a fixed local time (local noon) at different longitudes (45°W and 135°E), so they are from different universal times (UTs, 15UT and 3UT, respectively). Therefore, the difference between results in Figures 3&4 are not entirely longitudinal variations. It also includes effects of the UT variation. As the UT changes and the magnetic poles rotate around the geographic pole, the auroral Joule heating in both the hemispheres vary. Weimer et al. (2020) found that this UT variation of auroral Joule heating can cause substantiate variations in exosphere temperatures, especially in the polar regions: the maximum exosphere temperature occurred in the Southern polar region around 9 UT, in the Northern polar region at 21 UT, while the two poles are roughly equal at 3 UT and 15 UT. In this paper, 15 UT (Figure 3) and 3 UT (Figure 4) were chosen to minimize the UT effects and to underscore the longitudinal variations.

Latitudinal Dependency of the Equinox Transition

Whether during the December or June solstice seasons, the hemispheric O/N_2 differences increase with latitude, but the transition times between the two solstice seasons, the timings of the equinox transition, do not change much with latitude. This indicates that the rate of change in composition from one solstice season to the other is more dramatic at higher latitudes. Therefore, this aspect of the equinox transition is highly dependent on latitude.

Since upwelling decreases O/N_2 and downwelling increases O/N_2 , we can un-

derstand this latitudinal dependency by following the thermospheric circulation. On a daily average basis, the summer polar region has the largest solar heating, so upwelling is the largest, which causes larger decrease of O/N_2 at higher latitudes than at lower latitudes. This high latitude upwelling is further enhanced by the auroral Joule heating, which is present even at geomagnetically quiet periods (Cai et al., 2020, 2021). As the meridional wind encounters the EIA, it is suppressed in the summer hemisphere but accelerates after it passes the EIA in the winter hemisphere (Qian et al., 2016a). The wind then converges due to auroral Joule heating, producing large O/N_2 at subauroral latitudes.

The lower atmosphere can also contribute to the latitudinal dependency of the summer-to-winter difference in O/N_2 . Seasonal and latitudinal variations in wave/tidal activity, turbulent mixing, and residual circulations in the mesosphere and lower thermosphere region strongly impact the seasonal and latitudinal variations of thermosphere composition (e.g., Yamazaki and Richmond, 2013; Jones et al., 2014, 2017; Wu et al., 2017). For example, the lower thermospheric residual circulation reduces the summer-to-winter gradient of O/N_2 (Qian and Yue, 2017).

Note that GOLD O/N_2 shows a double low feature at mid to mid-high latitudes in the northern hemisphere during the June solstice season (52.5°N in Figure 2a, 42.5° and 52.5° in Figure 2c). NRLMSISE-00 O/N_2 does not have this double low feature (Figures 3 & 4). More observations and modeling work are needed to determine the nature of this double low feature during the June solstice season.

1. Conclusions

We compare GOLD O/N_2 with O/N_2 from GUVI and NRLMSISE-00 for consistency focusing on the seasonal time scale. We further characterize the latitudinal variability of the seasonal variation from low-mid to mid-high latitudes at a fixed local time and a fixed longitude using O/N_2 from GOLD and NRLMSISE-00.

We found that the overall seasonal/latitudinal patterns of O/N_2 in the GOLD, GUVI, and NRLMSISE-00 are consistent: an annual variation with a summer low and a winter high in O/N_2 at higher latitudes. The winter high O/N_2 at higher latitudes in one hemisphere transitions to winter high at higher latitudes in the other hemisphere through the equinoxes and lower latitudes, yielding seasonal variations at different latitudes with different annual and semiannual components.

There is a hemispheric asymmetry in the seasonal variation patterns: in the southern hemisphere, the seasonal variations exhibit the well-known annual and seminal pattern, with the highs near the equinoxes, and primary and secondary lows near the solstices. In the northern hemisphere, the seasonal pattern is dominated by an annual variation, with a minor semiannual component with the highs shifting away from the equinoxes towards the wintertime.

In addition, the characteristics associated with the equinox transition, includ-

ing the durations of the December and June solstice seasons, the magnitudes of the O/N_2 differences between the two hemispheres, and the downwelling convergence latitudes, are highly variable with longitude. Our hypothesis is that the EIA ion-neutral collisional heating, ion drag, and auroral Joule heating play substantial roles in determining the longitudinal dependence of these characteristics.

Finally, the rate of change in O/N_2 from one solstice season to the other is more dramatic at higher latitudes. Therefore, the equinox transition is also highly dependent on latitude.

Future work involves in using numerical model simulations to investigate physical mechanisms of the hemispheric asymmetry in the seasonal variation patterns, and the longitudinal and latitudinal dependencies of the equinox transitions.

Acknowledgments This study is supported by NASA grants 80NSSC20K0189, 80NSSC19K0278, 80NSSC18K0648, NNH19ZDA001N-HGIO, 80NSSC19K0835, NNH19ZDA001N-HSR, NNH19ZDA001N-HTMS and 80NSSC21K1315. This study is also supported by NASA contract 80GSFC18C0061 to the University of Colorado. The National Center for Atmospheric Research is a major facility sponsored by the National Science Foundation under Cooperative Agreement No. 1852977. GOLD O/N_2 are available online at <http://gold.cs.ucf.edu/search/>. GUVI O/N_2 are available at: http://guvitimed.jhuapl.edu/data_products. The data used to produce the figures in this paper are available at <https://doi.org/10.5065/p3wa-1q97>.

References

- Bowman B. R. (2004), The semiannual Thermosphere Density Variation From 1970 to 2002 Between 200-1100km, AAS 2004-174, AAS/AIAA Spaceflight Mechanics Meeting, Maui, Hi, February. Davies, K. (1990), Ionospheric Radio, Peter Peregrinus, London.
- Burns, A. G., S. C. Solomon, W. Wang, L. Qian, Y. Zhang, and L. J. Paxton (2012), Daytime climatology of ionospheric NmF2 and hmF2 from COSMIC data, *J. Geophys. Res.*, *117*, A09315, doi:10.1029/2012JA017529.
- Cai, X., Burns, A. G., Wang, W., Qian, L., Solomon, S. C., Eastes, R. W., et al. (2020). The two-dimensional evolution of thermospheric $\Sigma O/N_2$ response to weak geomagnetic activity during solar-minimum observed by GOLD. *Geophysical Research Letters*, *47*, e2020GL088838. <https://doi.org/10.1029/2020GL088838>
- Cai, X., Burns, A. G., Wang, W., Qian, L., Pedatella, N., Coster, A., et al. (2021). Variations in thermosphere composition and ionosphere total electron content under “geomagnetically quiet” conditions at solar-minimum. *Geophysical Research Letters*, *48*, e2021GL093300. <https://doi.org/10.1029/2021GL093300>
- Christensen, A. B., L. J. Paxton, S. Avery, J. Craven, G. Crowley, D. C.

- Humm, H. Kil, R. R. Meier, C.-I Meng, D. Morrison, B. S. Ogorzalek, P. Straus, D. J. Strickland, R. M. Swenson, R. L. Walterscheid, B. Wolven, and Y. Zhang (2003), Initial observations with the Global Ultraviolet Imager (GUVI) in the NASA TIMED satellite mission, *J. Geophys. Res.*, *108* (A12), 1451, doi:10.1029/2003JA009918.
- Correira, J., Evans, J. S., Lumpe, J. D., Krywonos, A., Daniell, R., Veibell, V., et al. (2021). Thermospheric composition and solar EUV flux from the Global-scale Observations of the Limb and Disk (GOLD) mission. *Journal of Geophysical Research: Space Physics*, *126*, e2021JA029517. <https://doi.org/10.1029/2021JA029517>
- Eastes, R. W., McClintock, W. E., Burns, A. G., Anderson, D. N., Andersson, L., Codrescu, M., et al. (2017). The Global-Scale Observations of the Limb and Disk (GOLD) mission. *Space Science Reviews*, *212*(1-2), 383–408. <https://doi.org/10.1007/s11214-017-0392-2>
- Eastes, R. W., McClintock, W. E., Burns, A. G., Anderson, D. N., Andersson, L., Aryal, S., et al. (2020). Initial Observations by the Global-scale Observations of the Limb and Disk (GOLD) mission. *Journal of Geophysical Research: Space Physics*, *125*, e2020JA027823. <https://doi.org/10.1029/2020JA027823>
- Emmert, J. T., and J. M. Picone (2010), Climatology of globally averaged thermospheric mass density, *J. Geophys. Res.*, *115*, A09326, doi:10.1029/2010JA015298.
- Fuller-Rowell, T. J. (1998), The “thermospheric spoon”: A mechanism for the semiannual density variation, *J. Geophys. Res.*, *103*, 3951-3956.
- Jones, M., Jr., J. M. Forbes, and M. E. Hagan (2014), Tidal-induced net transport effects on the oxygen distribution in the thermosphere, *Geophys. Res. Lett.*, *41*, 5272–5279, doi:10.1002/2014GL060698.
- Jones, M., Emmert, J. T., Drob, D. P., & Siskind, D. E. (2017). Middle atmosphere dynamical sources of the semiannual oscillation in the thermosphere and ionosphere. *Geophysical Research Letters*, *44*, 12–21. <https://doi.org/10.1002/2016GL071741>
- Lei, J., T. Matsuo, X. Dou, E. Sutton, and X. Luan (2012), Annual and semiannual variations of thermospheric density: EOF analysis of CHAMP and GRACE data, *J. Geophys. Res.*, *117*, A01310, doi:10.1029/2011JA017324.
- Paetzold, H. K., and H. Zschörner (1961), An annual and a semiannual variation of the upper air density, *Pure Appl. Geophys.*, *48*, 85.
- Paxton, L. J., et al. (1999), Global ultraviolet imager (GUVI): Measuring composition and energy inputs for the NASA Thermosphere Ionosphere Mesosphere Energetics and Dynamics (TIMED) mission, in *SPIE Optical Spectroscopic Techniques and Instrumentation for Atmospheric and Space Research III*, vol. 3756, 265-276, SPIE, Bellingham, Wash.

- Pilinski, M. D., and G. Crowley (2015), Seasonal variability in global eddy diffusion and the effect on neutral density, *J. Geophys. Res. Space Physics*, 120, 3097–3117, doi:10.1002/2015JA021084.
- Picone, J. M., A. E. Hedin, D. P. Drob, and A. C. Aikin (2002), NRLMSISE-00 empirical model of the atmosphere: Statistical comparisons and scientific issues, *J. Geophys. Res.*, 107, A12, 1468, doi:10.1029/2002JA009430.
- Qian, L., S. C. Solomon, and T. J. Kane (2009), Seasonal variation of thermospheric density and composition, *J. Geophys. Res.*, 114, A01312, doi:10.1029/2008JA013643.
- Qian, L. and S. C. Solomon (2011), Thermospheric Density: An Overview of Temporal and Spatial Variations, *Space Science Reviews*, doi:10.1007/s11214-011-9810-z.
- Qian, L., A. G. Burns, S. C. Solomon, and W. Wang (2013), Annual/semiannual variation of the ionosphere, *Geophys. Res. Lett.*, 40, 1928–1933, doi:10.1002/grl.50448.
- Qian, L., A. G. Burns, B. A. Emery, B. Foster, G. Lu, A. Maute, A. D. Richmond, R. G. Roble, S. C. Solomon, and W. Wang (2014), The NCAR TIE-GCM: A Community Model of the Coupled Thermosphere/Ionosphere System, American Geophysical monograph, 10.1029/2012GM001297.
- Qian, L., A. G. Burns, W. Wang, S. C. Solomon, Y. Zhang, and V. Hsu (2016a), Effects of the equatorial ionosphere anomaly on the interhemispheric circulation in the thermosphere, *J. Geophys. Res. Space Physics*, 121, 2522–2530, doi:10.1002/2015JA022169.
- Qian, L., A. G. Burns, W. Wang, S. C. Solomon, and Y. Zhang (2016b), Longitudinal variations of thermospheric composition at the solstices, *J. Geophys. Res. Space Physics*, 121, doi:10.1002/2016JA022898.
- Qian, L., and J. Yue (2017), Impact of the lower thermospheric winter-to-summer residual circulation on thermospheric composition, *Geophys. Res. Lett.*, 44, doi:10.1002/2017GL073361.
- Reigber, C., Balmino, G., Schwintzer, P., Biancale, R., Bode, A., Lemoine, J.M., Koenig, R., Loyer, S., Neumayer, H., Marty, J.C., Barthelmes, F., and Perossanz, F., 2002. A high quality global gravity field model from CHAMP GPS tracking data and accelerometry (EIGEN-1S). *Geophysical Research Letters*, 29(14), doi:http://dx.doi.org/10.1029/2002GL015064.
- Richmond, A. D., E. C. Ridley, and R. G. Roble (1992), A thermosphere/ionosphere general circulation model with coupled electrodynamics, *Geophys. Res. Lett.*, 19, 601.
- Rishbeth, H., and I. C. F. Müller-Wodarg (1999): Vertical circulation and thermospheric composition: a modelling study, *Ann. Geophys.*, 17, 794–805.

- Rishbeth, H., I. C. F. Müller-Wodarg, L. Zou, T. J. Fuller-Rowell, G. H. Millward, R. J. Moffett, D. W. Idenden, and A. D. Aylward (2000), Annual and semiannual variations in the ionospheric F2-layer: II. Physical discussion, *Ann. Geophys.*, *18*, 945–956
- Roble, R. G., E. C. Ridley, A. D. Richmond, R. E. Dickinson (1988), A coupled thermosphere/ionosphere general circulation model, *Geophys. Res. Lett.*, *15*, 1325.
- Tapley, B. D., Bettadpur, S., Watkins, M., and Reigber, C., 2004. The gravity recovery and climate experiment: mission overview and early results. *Geophysical Research Letters*, **31**(9), L09607, doi:<http://dx.doi.org/10.1029/2004GL019920>. American Geophysical Union.
- Weimer, D. R., Mehta, P. M., Tobiska, W. K., Doornbos, E., Mlynczak, M. G., Drob, D. P., & Emmert, J. T. (2020). Improving neutral density predictions using exospheric temperatures calculated on a geodesic, polyhedral grid. *Space Weather*, *18*, e2019SW002355. <https://doi.org/10.1029/2019SW002355>
- Wu, Q., Schreiner, W. S., Ho, S.-P., Liu, H.-L., & Qian, L. (2017). Observations and simulations of eddy diffusion and tidal effects on the semiannual oscillation in the ionosphere. *J. Geophys. Res. Space Physics*, *122*. <https://doi.org/10.1002/2017JA024341>
- Yamazaki, Y., and A. D. Richmond (2013), A theory of ionospheric response to upward-propagating tides: Electrodynamical effects and tidal mixing effects, *J. Geophys. Res. Space Physics*, *118*, 5891–5905, doi:10.1002/jgra.50487.
- Yu, T., Ren, Z., Le, H., Wan, W., Wang, W., & Cai, X., et al. (2020). Seasonal variation of O/N₂ on different pressure levels from GUVI limb measurements. *Journal of Geophysical Research: Space Physics*, *125*, e2020JA027844. <https://doi.org/10.1029/2020JA027844>
- Yue, J., Jian, Y., Wang, W., Meier, R. R., Burns, A., Qian, L., et al. (2019). Annual and semiannual oscillations of thermospheric composition in TIMED/GUVI limb measurements. *Journal of Geophysical Research: Space Physics*, *124*. <https://doi.org/10.1029/2019JA026544>
- Zeng, Z., A. Burns, W. Wang, J. Lei, S. Solomon, S. Syndergaard, L. Qian, and Y.-H. Kuo (2008), Ionospheric annual asymmetry observed by the COSMIC radio occultation measurements and simulated by the TIEGCM, *J. Geophys. Res.*, *113*, A07305, doi:10.1029/2007JA012897.
- Zhang, Y., L. J. Paxton, D. Morrison, B. Wolven, H. Kil, C.-I. Meng, S. B. Mende, and T. J. Immel (2004), O/N₂ changes during 1-4 October 2002 storms: IMAGE SI-13 and TIMED/GUVI observations, *J. Geophys. Res.*, *109*, A10308, doi:10.1029/2004JA010441.
- Zhang, S.-R., Holt, J. M., van Eyken, A. P., McCready, M., Amory-Mazaudier, C., Fukao, S., & Sulzer, M. P. (2005). Ionospheric local model and climatology

from long-term databases of multiple incoherent scatter radars. *Geophysical Research Letters*, 32(20), 9481. <http://doi.org/10.1029/2005GL023603>

Zhang, S.-R., Holt, J. M., van Eyken, A. P., Heinselman, C., & McCready, M. (2010). IPY observations of ionospheric yearly variations from high- to middle-latitude incoherent scatter radars. *Journal of Geophysical Research*, 115(A3), A03303. <http://doi.org/10.1029/2009JA014327>

Figure Captions

Figure 1: Comparisons of O/N_2 from GOLD, GUVI, and NRLMSISE-00 at the intersection of the GOLD FOV and GUVI orbits from October 2019 to September 2021. (a) GOLD; (b) GUVI; (c) NRLMSISE-00; (d) F10.7 (black line) and Kp (red line) indices. The local times shown in (b) is the GUVI sampling local times.

Figure 2: Seasonal variations of O/N_2 at noon and 45°W from October 2019 to September 2021, observed by GOLD: (a) time series of O/N_2 at 52.5°N (green), 42.5°N (brown), 32.5°N (red), 22.5°N (green); (b) time series of O/N_2 at 52.5°S (green), 42.5°S (brown), 32.5°S (red), 22.5°S (green); (c) time series of O/N_2 differences between pairs of northern hemisphere latitudes and the corresponding southern hemisphere latitudes. Green: 52.5°; brown: 42.5°; red: 32.5°; blue: 22.5°.

Figure 3: same as Figure 2 except that the results are from NRLMSISE-00.

Figure 4: same as Figure 2 except that the results are from NRLMSISE-00 at 135°E.